Angiboust, S., Kirsch, J., Oncken, O., Glodny, J., Monié, P., Rybacki, E. (2015): Probing the transition between seismically coupled and decoupled segments along an ancient subduction interface. - *Geochemistry Geophysics Geosystems (G3)*, *16*, 6, p. 1905-1922.

DOI: http://doi.org/10.1002/2015GC005776

AGU PUBLICATIONS

Geochemistry, Geophysics, Geosystems

RESEARCH ARTICLE
10.1002/2015GC005776

Probing the transition between seismically coupled and decoupled segments along an ancient subduction interface

Samuel Angiboust[1], Josephine Kirsch[1], Onno Oncken[1], Johannes Glodny[1], Patrick Monié[2], and Erik Rybacki[1]

[1]GFZ German Research Centre for Geosciences, Potsdam, Germany, [2]Geosciences Montpellier, UMR CNRS 5243, Université Montpellier 2, Montpellier, France

Key Points:
- The Dent Blanche Thrust is an ancient subduction interface from depths of ~35 km
- High-pressure foliated cataclasites and veins reveal deep brittle-ductile switches
- In situ image of fluid-rock interactions and deformation processes in this region

Supporting Information:
- Supporting Information S1
- Table S2
- Table S3
- Table S4

Correspondence to:
S. Angiboust,
samuel@gfz-potsdam.de

Citation:
Angiboust, S., J. Kirsch, O. Oncken, J. Glodny, P. Monié, and E. Rybacki (2015), Probing the transition between seismically coupled and decoupled segments along an ancient subduction interface, *Geochem. Geophys. Geosyst.*, *16*, 1905–1922, doi:10.1002/2015GC005776.

Received 13 FEB 2015
Accepted 1 JUN 2015
Accepted article online 3 JUN 2015
Published online 21 JUN 2015

Abstract The transition zone at the downdip end of seismic coupling along subduction interfaces is often the site of megathrust earthquake nucleation and concentrated postseismic afterslip, as well as the focus site of episodic tremor and slip features. Exhumed remnants of the former Alpine subduction zone found in the Swiss Alps allow analyzing fluid and deformation processes near the transition zone region (30–40 km paleodepth). The Dent Blanche Thrust (DBT) is a lower blueschist-facies shear zone interpreted as a fossilized subduction interface where granitic mylonites overlie a metamorphosed accretionary wedge. We report field observations from the DBT region where multiple, several tens of meters thick foliated cataclastic networks are interlayered within the basal DBT mylonites. Petrological results and microstructural observations indicate that the various cataclasis events took place at near-peak metamorphic conditions (400–500°C, 1.1–1.3 GPa) during subduction of the Tethyan seafloor in Eocene times (42–48 Ma). Some of these networks exhibit mutual crosscutting relationships between mylonites, foliated cataclasites, and vein systems indicating mutual overprinting between brittle deformation and ductile creep. Whole-rock chemical compositions, in situ ^{40}Ar-^{39}Ar age data of recrystallized phengite, and Sr isotopic signatures reveal that DBT rocks also underwent multiple hydrofracturing and metasomatic events via the infiltration of fluids mainly derived from the oceanic metasediments underneath the DBT. From the rock fabrics, we infer strain rate fluctuations of several orders of magnitude beyond subduction strain rates ($\sim 10^{-12}$ s^{-1}) accompanied by fluctuation of supralithostatic and quasi-lithostatic fluid pressures ($1 \geq \lambda > 0.95$). DBT brittle-plastic deformation switches highlight the diversity of deformation processes and fluid-rock interactions in the transition zone region of the subduction interface.

1. Introduction

The subduction interface, which exhibits a wide diversity in terms of deformation patterns, is commonly divided in two main segments which may partially overlap in time and space: the seismogenic zone and the decoupled, creeping interface toward depth. The seismogenic zone, generally located between 10 and 35 km depth depending on slab dip and thermal structure (i.e., between temperatures of 150°C and 350–450°C), corresponds to a portion of the interface subject to strong mechanical coupling where devastating megathrust earthquakes happen [e.g., *Tichelaar and Ruff*, 1993; *Oleskevich et al.*, 1999] (Figure 1). Locally, conditionally stable segments are subject to creep, while the frictionally unstable portions remain locked through most of the seismic cycle [e.g., *Scholz*, 1998]. Some studies also report the presence of partially unstable locked patches, which may potentially correspond to asperities along the subduction plane [e.g., *Ito et al.*, 2007]. At depths of 40 km and deeper, the mechanical properties of the interface dramatically change, most likely due to the entrance of subducted material within the subcontinental mantle and/or due to thermal activation of plastic deformation mechanisms above 450°C [e.g., *Oleskevich et al.*, 1999; *Wada and Wang*, 2009]. The formation of hydrous minerals (e.g., serpentine, talc, etc.) resulting from fluid infiltration from the dehydrating downgoing slab into the overlying mantle wedge is also believed to significantly promote aseismic behavior and to control the downdip limit of large thrust earthquakes in many subduction zones [e.g., *Peacock and Hyndman*, 1999] (Figure 1). This region of the plate interface is also subject to mechanical instabilities and "intermediate-depth" seismicity whose origin needs to be better understood [e.g., *Hacker et al.*, 2003; *Angiboust et al.*, 2012; *Andersen et al.*, 2014].

The nature of deformation at plate margins has been reconsidered in the last decade by a growing awareness of a variety of discontinuous deformation processes that exhibit a wide range of temporal scales from

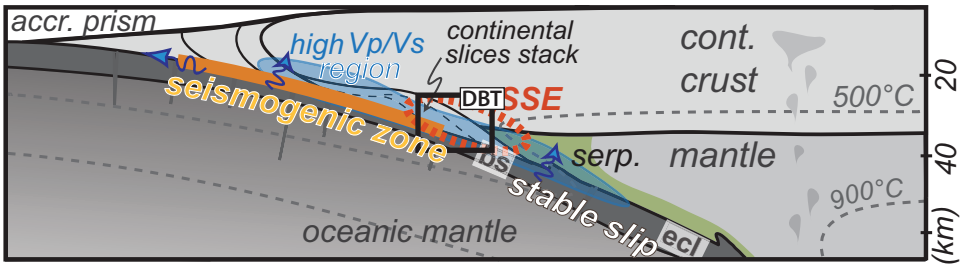

Figure 1. Simplified view of an oceanic subduction zone showing the location in blue of high Vp/Vs regions (indicating higher fluid contents) along the seismogenic zone, where the mechanical coupling is the highest. The dotted orange line localizes the region where SSE (Slow Slip Events) and ETS are generally observed. Blue arrows correspond to the regions of enhanced fluid transfer. The black rectangle (DBT: Dent Blanche Thrust region) corresponds to the geological structure observed in the field in the Alps and described in this manuscript. *serp.*: serpentinization of the mantle wedge. *bs*: lower bound of the blueschist-facies field; *ecl*: lower bound of the eclogite-facies field.

fast seismic shocks to long-term creep. An increasing number of GPS-based measurements and seismological observations led to the recognition of an unusual variety of features on many convergent margins: the episodic tremors and slow transients, often located along the subduction interface itself, near the transition between stick-slip and stable-sliding frictional regimes [*Rogers and Dragert*, 2003; *Liu and Rice*, 2007]. Pressure-Temperature conditions associated with these "slow slip phenomena" frequently range from 350°C to 600°C and 0.8 to 1.4 GPa (~20–40 km depth) depending on the subduction thermal gradient [e.g., *Peacock and Wang*, 1999; *Shelly et al.*, 2006; *Ito et al.*, 2007] (Figure 1). Previous studies have proposed that the release of accumulated elastic strain by slow slip phenomena may be temporally and spatially associated with an expected or recent major rupture along the seismogenic zone [e.g., *Ozawa et al.*, 2002]. Several studies also pointed out that slow slip phenomena exhibit seismic source characteristics which differ from regular earthquakes [e.g., *Shelly et al.*, 2006]. However, the exact location of these events, the nature of the processes governing these events and their relationships with megathrust earthquakes remain poorly known and debated [*Peng and Gomberg*, 2010].

The apparent match between the location of these unusual seismic events and the seismological evidence of elevated pore fluid pressure regions (as shown by Vp/Vs or Poisson's ratios) suggests the existence of a mechanical interplay between fluids and slow slip generation [*Audet et al.*, 2009]. The location of these high pore fluid pressure anomalies seems to be variable in time and related to the different stages of the seismic cycle, thus supporting the hypothesis of the presence of a dynamically coupled hydromechanical system [e.g., *Kodaira et al.*, 2004; *Frank et al.*, 2015]. Even though some studies propose that slow slip phenomena should occur on a large, continuous, and fluid saturated fault zone with high-permeability anisotropies [e.g., *Peacock et al.*, 2011], these interpretations remain qualitative and difficult to constrain with direct observations.

We herein describe a major Alpine shear zone, the Dent Blanche Thrust (DBT), which has recently been interpreted as a fossilized subduction interface at depths of ~35 km [*Angiboust et al.*, 2014a]. The first report of high-pressure brittle deformation patterns along the hanging wall of this contact, at depths where plastic deformation normally dominates provides critical information on deformation regimes and rock-fluid interaction processes operating along the "transition zone," i.e., at the junction between seismically coupled and decoupled segments of the subduction interface.

2. Geological Setting

The Central Alps in Southern Switzerland, where segments of the Alpine subduction channel are preserved, expose the tectonic contact along which orthogneisses from the Apulian microcontinent (upper plate) were thrusted upon the remnants of the Tethyan seafloor (dominantly accreted oceanic metasediments from the subducting oceanic lower plate; Figure 2a) [*Marthaler and Stampfli*, 1989; *Bachmann et al.*, 2009]. In the Dent Blanche region, this metamorphosed accretionary complex (named "Tsaté oceanic complex" in this locality) and the overlying Arolla gneisses of Apulian affinity have been both subducted down to 25–40 km depths (Figures 2a and 2b). Geochronological investigations have shown that the 2–3 km thick slice of Arolla orthogneisses, which has been underplated to the upper plate material at circa 58 Ma, continuously occupied a subduction interface hanging wall position between 58 and 43 Ma [*Angiboust et al.*, 2014a] (Figure 2b).

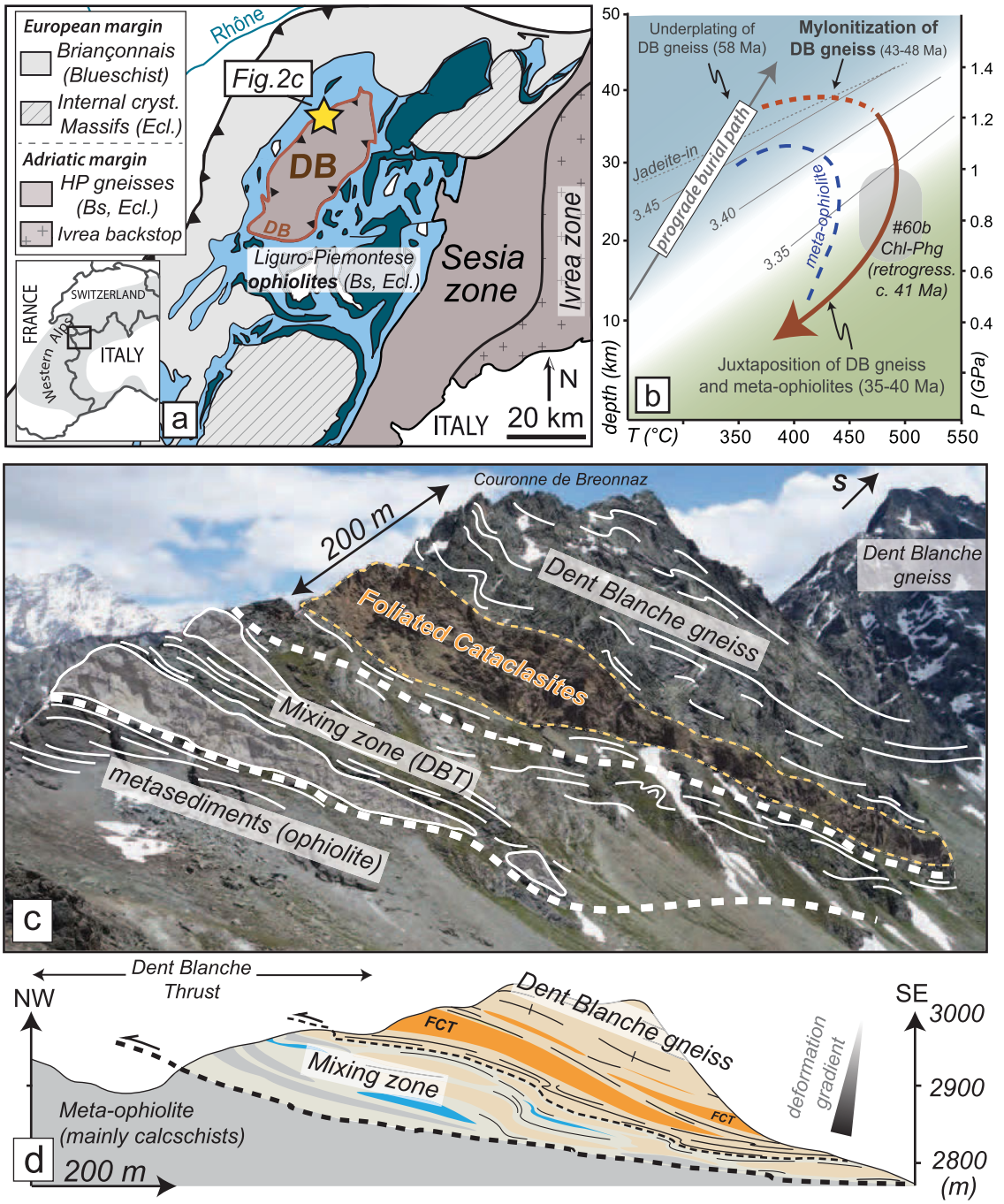

Figure 2. (a) Simplified geological map of the Northwestern part of the Alpine belt showing the location of the Dent Blanche tectonic system (DB) and its lateral equivalent, the Sesia zone. Its basal contact, highlighted in red, is named Dent Blanche Thrust (DBT) in this study and is considered as an ancient subduction interface, juxtaposing continental gneiss with metaophiolites derived from the Liguro-Piemontese seafloor. Light blue: metasediments; dark blue: mafics and ultramafic bodies. (b) Pressure-Temperature-time path followed by Dent Blanche gneisses (Arolla unit) and by the underlying metasediments from the Tsaté complex (thermobarometric and pseudosection modeling data from *Angiboust et al*. [2014a]; prograde burial path from *Agard et al*. [2001]). Blue-shaded and green-shaded areas correspond to blueschist (i.e., blue-amphibole bearing domain) and greenschist facies, respectively [see also *Evans*, 1990]. (c) Field view of the DBT in the region of Moiry lake (Switzerland), showing the Dent Blanche mylonitic gneiss overlying a mixing zone where slivers of both continental and oceanic affinities are tectonically intermixed. The main layer of foliated cataclasites, which reaches nearly 100 m in thickness in this region, is located near the base of the mylonites, close to the tectonic mixing zone. (d) Idealized sketch of the Couronne de Breonnaz crest showing the simplified tectonic structure and the existence of several foliated cataclastic networks crosscutting the base of Arolla gneiss mylonites. A deformation gradient increasing from the base toward the center of Arolla gneiss is visible on the field on the scale of several hundred meters. Blue lenses: marbles. Pale yellow: foliated greenschists and phyllonites. Rare, meter-sized serpentinite slivers are occasionally visible along this cross section (not shown here).

This deformation age spread, along with the tremendous shearing recorded by the ~500 m thick mylonitic DBT shear zone at the base of the Arolla slice both point to a long-lived velocity gradient associated with ongoing subduction of the Tethyan oceanic lithosphere.

The lowermost part of the DBT (Figures 2c and 2d) is often characterized by the presence of a complex tectonic mixing zone involving strongly flattened slices of both continental and oceanic material. The upper contact to the mixing zone below the base of the Arolla unit (see Figure 2c) is sharp and only a few cm wide. This mixing zone reaches ~150 m in thickness in the Couronne de Breonaz area. It contains flattened lenses of serpentinite, greenschists, gneissic basement fragments as well as quartzites, calcschists, and marbles. These lenses range in thickness from several meters to tens of meters, and are embedded within a strongly schistose matrix where greenschists and metapelites dominate.

The underlying oceanic domain (Tsaté complex) is dominantly composed of calcschists and metapelites with minor amounts (<20 vol %) of mafic and ultramafic lenses. Tsaté complex regional foliation, generally trending subparallel to the DBT, is affected by large amplitude NW-SE megafolds. Tsaté complex structure comprises various km sized slices having experienced slightly different P-T-t paths during subduction and complex underplating processes within the Alpine subduction channel [*Angiboust et al*., 2014a]. Maximum temperatures span a range between 360 and 490°C, corresponding to maximum burial depths of 25–40 km (calculated using the geothermal gradient value of 8°/km commonly considered for the W. Alps subduction zone; Figure 2b). Quartz and calcite veins, boudinaged, stretched, and reoriented are very frequent in metasedimentary lithologies. Both quartz and calcite exhibit a crystal-plastic behavior while albite clasts remain undeformed throughout the Alpine metamorphic history. Pressure solution fringes are systematically observed along the main foliation in pelitic and carbonated metasedimentary rocks [*Ring*, 1995; *Angiboust et al*., 2014a].

Foliation trends and stretching lineations are similar within Arolla gneisses, the DBT mixing zone and in the underlying oceanic domain. The deformation sequence is dominated by two major events: a first top-to-NW, high-pressure shearing event interpreted to have formed during the subduction event (e.g., Figure 3a) followed by a lower-pressure tectonic overprint of moderate importance and heterogeneous spatial distribution. This late event, characterized by crenulation folds visible at all scales and by top-to-SE kinematic indicators, is particularly intense in the mechanically weaker Tsaté oceanic complex [*Ring*, 1995; *Angiboust et al*., 2014a]. The temperature difference between the mixing zone calcschists (350–450°C) and Arolla gneisses (450–500°C) suggests that tectonic juxtaposition between Tsaté complex and Arolla unit occurred lately in the DBT deformation history [*Angiboust et al*., 2014a]. This observation, supported by Rb-Sr deformation ages younger than Arolla gneisses ages, highlights the complex metamorphic history of the mixing zone, which should not be viewed as the pristine footwall of the DBT. The total amount of subduction-related strain recorded by Arolla mylonites and cataclasites is several orders of magnitude higher than the backshear which led to the present-day juxtaposition [see *Ballèvre and Merle*, 1993; *Wheeler and Butler*, 1993; *Ring*, 1995]. The ubiquitous superposition of upper plate material against accretionary wedge material for more than 200 km from the DBT region to eastern Switzerland and western Austria (e.g., Arosa zone) [*Bachmann et al*., 2009] also supports the idea that the late backshear regionally observed only moderately reworked the prevalent primary structures, inherited from the subduction stage. This backshear overprint is associated with incipient collisional deformation during entrance and subsequent exhumation of the European margin ("Briançonnais") in the Alpine subduction zone between 42 and 38 Ma (Figure 2a) [*Mazurek*, 1986; *Wust and Silverberg*, 1989; *Pennacchioni and Guermani*, 1993; *Gebauer*, 1999; *Rosenbaum et al*., 2012; *Angiboust et al*., 2014a].

3. Material and Methods

We sampled 40 hand specimens of DBT gneisses from three different locations for bulk-rock analysis and thin section observations. Detailed information regarding sampling, analytical measurements, and procedures are given in supporting information. Electron Probe Microanalysis on individual minerals (only phengite and epidote/clinozoisite chemical data are presented here) from fabric A and B rocks have been performed at GFZ Potsdam following the procedure described in Data set S1. Major elements whole-rock analyses have been performed by X-Ray Fluorescence (XRF) at GFZ Potsdam (Data set S2). In order to characterize the source of fluids present during the multiple stages of deformation identified in this study, a suite of foliated cataclasites and epidote-rich vein material has been selected for $^{87}Sr/^{86}Sr$ isotopic signature characterization (Data set S3). In situ $^{40}Ar/^{39}Ar$ laser ablation dating has been performed at Montpellier University on two polished rock sections (Data set S4).

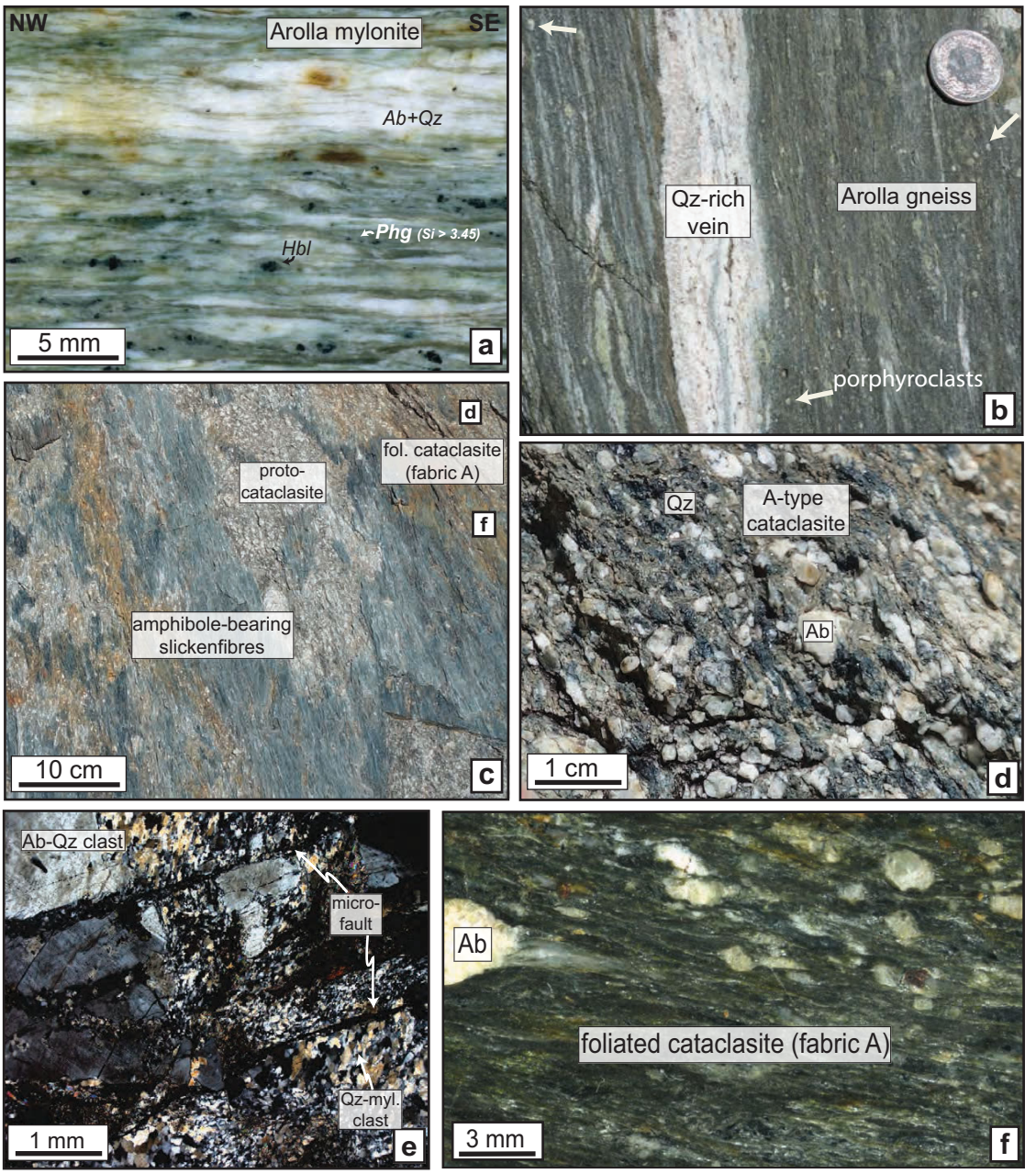

Figure 3. (a) Polished rock slab representative for the structure of the Arolla gneiss, high-pressure mylonitic foliation [*Angiboust et al.*, 2014a]. (b) Field view showing a quartz-rich vein cutting through the proto-cataclastic matrix (fabric A) representative of semibrittle deformation within the DBT hanging wall (Arolla region). Note the presence of numerous millimeter-sized quartz and albite clasts aligned along the foliation (white arrows). (c) Field view showing slickenline fibers networks cutting through the protocataclastic fabric A. High-silica phengites (Si = 3.5 p.f.u), blue and blue-green amphiboles (up to 6.5 wt % Na_2O: Mg-riebeckites) are both present in the fibers and in the surrounding matrix. (d) Field view showing the A-type cataclastic structure showing angular clasts of quartz and albite within a weakly foliated, phengite-amphibole-quartz-bearing matrix. (e) Optical microscope view of a proto-cataclasite sample showing incipient fracturing of the Arolla mylonitic matrix. Note that grain boundaries in mylonite clasts are preferentially aligned and subparallel. (f) Polished rock slab showing the internal structure of a B-type foliated cataclasite in which clasts of albite and quartz float in a Phg, Mg-Rbk, Ttn (Rt), Qz, Py, Chl ± Ep foliated domain (Arolla-Monts Dolins region; sample #100c).

4. Observations and Results

4.1. Field Relationships in the Dent Blanche Thrust Region

The lowermost DBT mylonites exhibit for more than 35 km along-strike in Switzerland a wide continuum of foliated rocks comprising finely banded mylonites (Figure 3a), porphyroclastic mylonites (Figure 3b), and DBT-parallel domains (fabrics A and B) ranging from ~1 to ~100 m in thickness. The first type (fabric A), particularly well expressed in the Arolla region, exhibits heterogeneously fragmented decameter-thick proto-cataclastic

domains (i.e., with 10–50 vol % matrix) locally grading to centimeter-thick cataclastic networks (50–90 vol % matrix) in which albite and quartz-albite microfractured aggregates are floating in a variably penetrative foliation (Figures 3c–3f; see also E. Strøm, Petrography, deformation and metamorphism of the Arolla Cross section, SW Switzerland, unpublished MS thesis, University of Oslo, 1990). Some of these networks are locally intersected by foliation-subparallel, bluish slickenfibers (Figure 3c) containing numerous millimeter-sized pyrite crystals. It was neither possible in the field nor on microscopic scale to identify the dominant shear sense in an unequivocal manner within fabric A domains. Foliation-subparallel centimeter to decimeter-thick quartz-filled veins are also frequent in Arolla mylonites and also within fabric A facies (Figure 3b), in particular within the first 300 m above the DBT contact zone. The boundary between Arolla mylonites and fabric A domains seems continuous in the field. Importantly, neither pseudotachylite veins nor former injection textures have been observed along and above the DBT despite thorough investigations.

Fabric B (particularly thick and well preserved in the Couronne de Breonaz ridge; see the star in Figure 2a) forms decimeter-thick networks, which exhibit a strike and a dip generally parallel to the overlying DBT mylonites and to the basal contact of the DBT (Figure 2c). Due to the lack of large-scale continuous exposures, it is impossible to evaluate precisely the lateral extent of fabric A networks in the field (Figures 2c and 2d). Fabric B rocks, very different from A-type facies, typically comprise very finely banded foliated facies showing numerous microfolds, Arolla mylonite clasts and folded veins of various orientations (Figures 4a and 4b). Fabric B rocks also contain abundant millimeter-sized oxidized pyrite crystals, giving an orange-yellowish appearance to these domains in the field. Coarse-grained cataclastic textures as visible within fabric A domains (Figure 3d) were not observed within B-type domains. In the most sheared B-type facies, the matrix consists of homogeneous, fine-grained greyish levels, stripped by lighter yellowish to whitish veins intensely microfolded and strictly parallel to the main foliation. The strain recorded by these facies is much higher than for A-type fabrics and the boundary with the overlying Arolla mylonites is also sharper, on the order of several tens of centimeters. Both Arolla mylonites and B-type facies show primary top-to-NW kinematic criteria jointly affected by the above described late top-to-SE motion associated with late exhumation stages.

4.2. Petrological Description of DBT Rocks

Arolla mylonites in the DBT vicinity exhibit a pervasive planar deformation and often contain less than 15% porphyroclasts. Their mineralogy is relatively homogeneous and characterized by alternations of thin phyllosilicate-rich planes and thick quartz-albite segregates (Figure 3a). A moderate quartz *c* axis crystal preferred orientation is occasionally visible in quartz-rich layers, where the size of most grains range from 30 to 70 μm in diameter, presumably due to dynamic recrystallization processes during mylonitization (see supporting information for Electron Back-Scattered Diffraction imaging results). Phengite crystals lining the foliation are relatively large ($>$100 μm) and with high celadonite contents (corresponding to silica contents on the order of 3.5 p.f.u; Figure 5a; supporting information; see detailed petrology and chemical analyses in *Angiboust et al*. [2014a, and references therein]). Pyrite is rare in DBT mylonites ($<$0.1 vol %).

Pristine A-type facies in which typical coarse-grained cataclastic structures can be recognized are rather rare in the field (Figure 3d). Rupture, fragmentation, and mechanical comminution led to grain size reduction and dissemination of albite, quartz, and mylonite fragments (Figure 3e). In the most foliated facies, the cataclastic fabric cannot be clearly identified because these clasts were wrapped within a very fine-grained quartz-albite-phengite-chlorite-amphibole cohesive matrix (Figure 3f), systematically showing crystal-preferred orientation of quartz, phyllosilicates (when present) and abundant pressure-solution fringes. Phengite crystals observed in these lithologies, in textural equilibrium with magnesio-riebeckite crystals (blue amphibole; up to 6.5 wt % Na_2O), exhibit high silica contents of $\sim$3.5 p.f.u (Figure 5a; supporting information). Rutile is observed within titanite cores in fabric A matrix. Chlorite is found along the foliation between blue-amphibole and phengite crystals. Phengite from quartz-bearing veins cutting across Arolla orthogneisses (Figures 3a and 3b) exhibit celadonite-rich phengite compositions relatively close to the ones obtained for high-pressure mylonites (Si $\sim$ 3.4 p.f.u; sample #12L; supporting information). Many of these veins have been reoriented and flattened during ongoing mylonitic deformation.

Decimetric to decametric-sized mylonitic fragments of Arolla mylonites are occasionally preserved within B-type domains exposed along the DBT hanging wall (see Figures 2d and 4b). The very rare occurrences of nonfoliated B-type domains comprise a cohesive, fine-grained matrix with diverse mineral fragments and Arolla-type mylonitic clasts of various sizes (Figure 4c). These microstructural characteristics point to the existence of cataclastic deformation during shearing [*Sibson*, 1977]. Exposed B-type networks are more

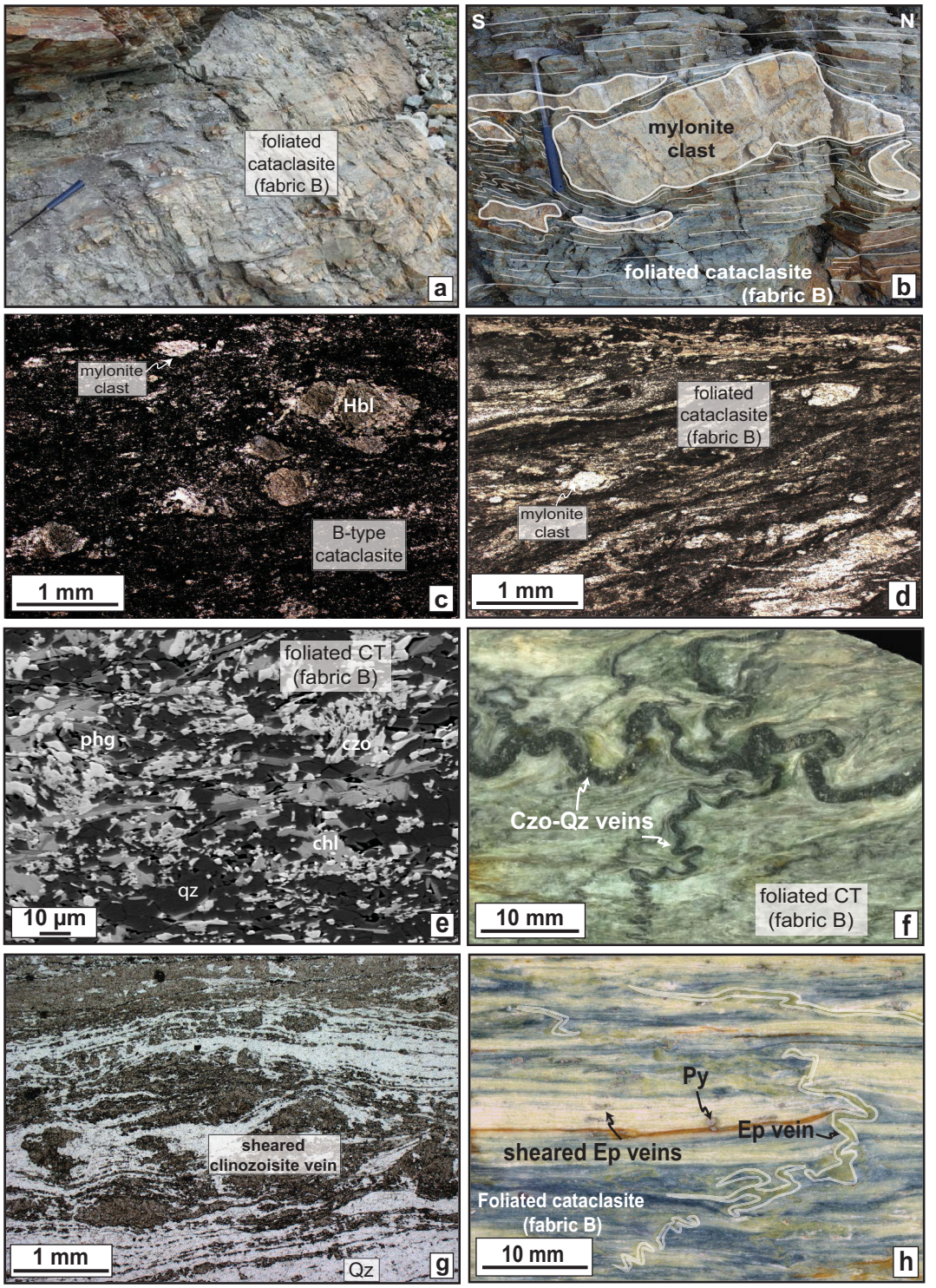

Figure 4. (a) Outcrop view showing the pervasive foliation affecting DBT B-type foliated cataclasites (hammer for scale: 40 cm long). (b) Outcrop view showing Arolla mylonite fragments sheared, folded, and wrapped in the foliated cataclasite matrix. (c) Optical microscope view (nonpolarized light) showing the structure of a B-type fabric were the cataclastic fabric has been preserved from postcataclasis shearing. (d) Optical microscope view showing a foliated cataclasite matrix where various-sized fragments of the previous mylonite are floating (fabric B). Note the abundance of dark fringes lining the foliation pointing to the presence of pressure-solution deformation processes. (e) Back-scattered electrons image representative for the small-scale structure of DBT foliated cataclasites (fabric B) where 10–20 μm wide clasts of phengite (phg), chlorite (chl), clinozoisite (czo), titanite, quartz (qz), and albite float in a weak, scaly foliation. (f) Photograph of a network of several generations of clinozoisite/quartz-rich veins cutting across the foliated cataclasite matrix (fabric B). (g) Optical microscope view showing former clinozoisite veins now reoriented along the main foliation. Note the pervasive ductile deformation affecting the quartz-rich layers. (h) Photography of a polished rock surface of a foliated cataclasite showing alternating epidote (Ep)-rich (yellowish) and quartz-richer layers (greyish), crosscut by strongly folded epidote-rich veins. Pyrite (Py) is very abundant in the rock matrix.

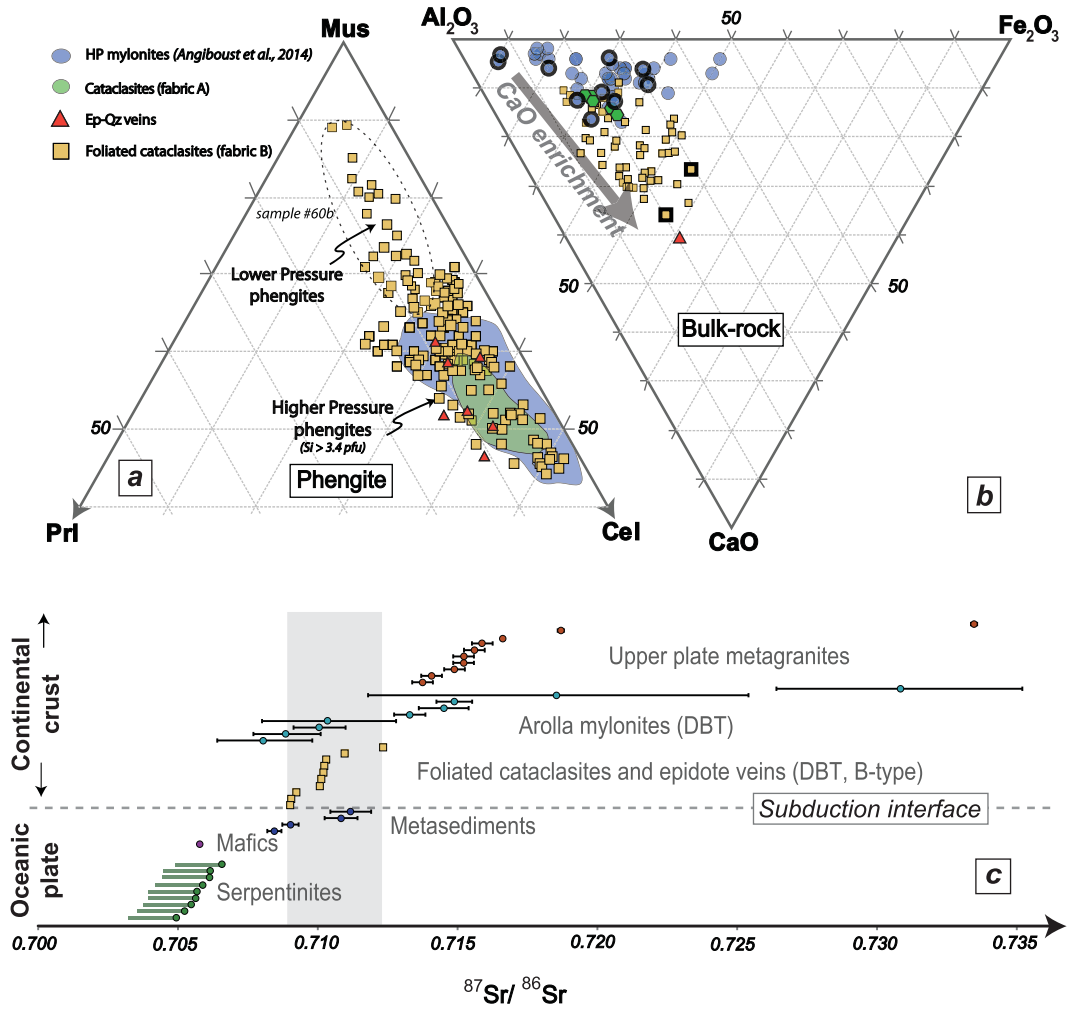

Figure 5. (a) Ternary plot of phengite composition (Prl: pyrophyllite; Cel: celadonite; Mus: muscovite) for mylonites and foliated cataclasite material collected along the DBT. This figure shows that phengite crystals from both A and B cataclasite types and vein material (from fabric B) have a composition which overlaps the composition of Arolla mylonite phengites formed during peak metamorphism [see also *Angiboust et al.*, 2014a]. (b) Ternary plot of bulk-rock composition estimates in the Aluminum-Calcium-Iron system showing compositions calculated from surface composition estimates at the Scanning Electron Microscope (thin line circles) and those measured by X-Ray Fluorescence whole-rock analysis (black thick line circles). Foliated cataclasites exhibit a marked CaO enrichment attesting to fluid-rock interaction during deformation along the DBT. (c) Summary of Sr isotopic compositions (recalculated for an age of 43 Ma) obtained for a variety of samples from the DBT region (metasediments, gneisses, foliated cataclasites, granitoids) and from mafic/ultramafic samples from the underlying oceanic Tsaté complex (complete data set and references given in supporting information).

often characterized by a penetrative and relatively scaly foliation, depending on deformation intensity, clast size, and frequency (Figure 4d). These domains are internally composed of a very fine-grained matrix of angular quartz, albite, epidote-clinozoisite, and titanite clasts ranging in size from 10 to 40 μm (Figure 4e). Millimeter-sized clasts of albite, hornblende pseudomorphs, and mylonitic material are sometimes preserved in the matrix, wrapped by the main foliation (Figure 4d). The proportion of clasts can be very variable at the centimeter scale (Figures 4c and 4d). These foliated cataclasites contain numerous dark fringes comprising small oxides and titanite porphyroclasts aligned along the foliation in the matrix or underlying tight folds. Rutile is frequently found as relicts within the largest titanite porphyroclasts. Phengite, chlorite, and actinolite are also present as minor phases ($<$1 vol % on average). Blue and blue-green amphibole which diagnostically characterizes fabric A deformation has not been observed within fabric B foliated cataclasites. The modal proportion of phengite is often lower in the foliated cataclasites than in the original mylonite. Phengite flakes are rare, small ($<$15 μm), and exhibit a wide range of silica contents comprised between 3.25 and 3.52 p.f.u (representative EPMA data set available in supporting Information). None of these

phengite clasts exhibit a zoning pattern. Foliated cataclasites showing a strong overprint by crenulation cleavage and SE-directed shearing have lower silica contents (Figure 5a; sample #60b).

Foliated cataclasites are crosscut by numerous yellowish to greyish veins ranging in thickness from 1 mm to 1 cm and up to 20 cm in length. When preserved from later pervasive ductile shearing, these folded veinlets are observed cutting across the main foliation at very variable angles (Figures 4f and 4h). Clinozoisite/epidote and quartz are the two dominant phases filling these veins. Epidote iron content is apparently slightly lower in B-type foliated cataclasites and associated veins (∼20 mol % pistacite component) than in Arolla mylonites (∼30 mol % pistacite component). Carbonates are rare within A-type and B-type fabrics. Some of the largest veins, sheared, and boudinaged via shearing, are now visible as dark blocky clasts wrapped by the foliation (supporting information). Ancient clinozoisite-rich veins can be recognized in the foliated cataclasite matrix by the presence of discontinuous yellow to greyish segments lining the main foliation (Figure 4f). These clinozoisite/epidote-rich domains can locally be as thick as several tens of centimeters in the largest foliated cataclasite layers. Fractures within clinozoisite-rich veins are systematically filled by quartz. Quartz segregates and phyllosilicate-rich layers from foliated cataclasites often exhibit a marked crystal-preferred orientation (visible using a gypsum plate on an optical microscope). Conversely, albite and clinozoisite clasts do not show clear evidence for plastic flow throughout DBT deformation history.

Crosscutting relationships between clinozoisite-quartz veins and the surrounding matrix indicate that cataclasis and vein opening took place sequentially via multiple events (Figure 4f). Field and microstructural observations indicate that the cataclastic matrix has been systematically cemented and reworked by a foliation resulting from solution-precipitation creep after cataclasis. The observation of a marked crystal-preferred orientation in both quartz-rich layers and phyllosilicate-rich layers suggests that dynamic recrystallization processes, along with subgrain rotation and high-angle grain boundary migration, played also an important role during shearing after cataclasis (Figure 4g).

4.3. Metamorphic History of DBT Foliated Cataclasites

In order to identify the part of the deformation history associated to the lower blueschist-facies subduction event, we tried to separate the various events that affected the DBT and focused on regions where the exhumation-related, greenschist-facies overprint is limited. The broad range covered by phengite celadonite content, which helps to constrain relative pressure changes [*Angiboust et al*., 2014a] (Figure 5a) and the fabrics identified as late stage deformation (crenulations, SE-directed shearing) can be used to identify these two main tectono-metamorphic stages. Recent Pressure-Temperature (P-T) estimates based on pseudosection modeling indicate that the main mylonitization stage (associated with top-to-NW kinematic indicators) along the DBT took place at about 1.2 GPa, ∼450°C [*Angiboust et al*., 2014a]. Phengite crystals from both fabrics A and B, reequilibrating during DBT deformation history, show celadonite contents nearly as high as for the mylonites, suggesting that cataclasis and mylonitization proceeded near-peak conditions depths (∼35 km; Figure 5a). The absence of intrasample zoning also suggests that phengite clasts systematically reequilibrated throughout DBT metamorphic history. The observation of a marked crystal-preferred orientation pattern of phengite-bearing layers in foliated cataclasites suggests that the complete reequilibration of former prograde phengite clasts was due to dynamic recrystallization processes. This reequilibration of phengite clasts was also probably permitted by (i) the extremely fine-grained clast size (<15 μm wide) and (ii) by the ubiquitous presence of pressure-solution processes, enhancing metamorphic reaction rates.

The high-pressure metamorphic memory of A-type cataclasites is often better preserved from exhumation-related metamorphic overprint than within fabric B foliated cataclasites lining the base of the DBT. P-T estimates on samples showing numerous top-to-SE kinematic indicators, exhibiting large chlorite amounts ($>$10 vol %) and abundant low-Si phengite crystals (Si = 3.2) indicate that the late tectonic and metamorphic reequilibration of fabric B cataclasites occurred near 500°C and 0.8 GPa (∼20 km depth; sample #60b [*Angiboust et al*., 2014a]) (Figures 2b and 5a).

Although detailed P-T conditions of clinozoisite-quartz vein formation are difficult to evaluate precisely, crosscutting relationships with surrounding foliated cataclasites (fabric B) together with high celadonite contents of the rare phengite crystals found within these veins also suggest P-T conditions of formation near the metamorphic peak (Figure 5a; supporting information).

4.4. Chemical Composition of DBT Cataclasites

In order to identify the existence of fluid-rock interaction processes and element mobility during deformation along the DBT, we performed a series of whole-rock XRF analysis of major elements for mylonites (10 samples) and fabric B foliated cataclasites (2 samples). These analyses were compared to surface composition analyses obtained using a Scanning Electron Microscope for both mylonites (34 analyses), fabric A (6 analyses), and fabric B foliated cataclasites (50 analyses). Chemical data obtained via both techniques are presented in Figure 5b in a triangle (see supporting information for chemical compositions data set). It shows that (i) fabric A foliated cataclasites are not significantly affected by fluid-rock interaction (ii) fabric B foliated cataclasites are more enriched in CaO than the protolith they derive from. Fabric B cataclasites exhibit compositions which tend to be closer to the composition obtained for the clinozoisite/epidote-rich, vein material (green triangle in Figure 5b). The K_2O content of fabric B foliated cataclasites (0.8 wt % on average) is also much lower than the one obtained for Arolla mylonites (2.7 wt %; supporting information).

4.5. Strontium Isotopes Characterization of DBT Rocks

The measurement of strontium isotopic ratio $^{87}Sr/^{86}Sr$ is a powerful tool to identify fluid-rock interaction or mixing of fluid sources in former subduction zone settings [e.g., *Glodny et al*., 2003]. In order to understand whether the fluid responsible for vein-filling originated from an external source, we performed a series of measurements on both vein material and foliated cataclasites and compared these results with strontium isotopic signatures from the other rock-types occurring on both sides of the DBT (see Figure 5c and supporting information for the complete data set). Our results show that the $^{87}Sr/^{86}Sr$ isotopic signature of foliated cataclasites and vein material (both part of fabric B) span a relatively restricted range comprised between 0.709 and 0.712. The range covered by Arolla mylonites and other granitoids derived from the Adriatic upper plate is broader and generally higher, between 0.708 and 0.737. Conversely, the range spanned by the metasediments from the underlying oceanic complex (mainly calcschists and metapelites) is narrower and comprised between 0.708 and 0.711. Strontium isotopic signatures of mafic and ultramafic rocks are systematically the lowest, with $^{87}Sr/^{86}Sr$ ratios often lower than 0.707.

4.6. Geochronological Constraints on Deformation Processes

Recent investigations on Arolla mylonites using Rb-Sr geochronology indicated that ductile deformation along the DBT proceeded over a long period of time, from (58) 50 to 43 Ma [*Angiboust et al*., 2014a] (Figure 6). Their Rb-Sr age of 46.9 ± 1 Ma obtained for an A-type cataclasite sample from the DBT (sample #100c; Figure 3d) shows that plastic (Arolla mylonites) and brittle deformation are contemporaneous. In order to bracket the timing of the brittle deformation observed along the DBT, we provide two new age constraints using in situ ^{40}Ar-^{39}Ar geochronology. Phengite crystals from foliated cataclasite samples (fabric B) were too small and too sparse to be analyzed via Rb-Sr or ^{40}Ar-^{39}Ar geochronology. However, one foliated cataclasite sample showing a strong greenschist-facies imprint (indicated by low-celadonite phengite compositions and high chlorite amounts) and sufficient phengite amounts have been successfully dated using ^{40}Ar-^{39}Ar geochronology (sample #60b; supporting information; Figure 5a). We also analyzed a quartz-phengite-chlorite bearing hydrofracture vein (sample #12L; supporting information) cutting across the Arolla mylonites in the Couronne de Breonaz region (Figure 2c). Despite some dispersion, the average of 12 laser point analyses on phengite crystals from the hydrofracture vein #12L provides metamorphic ages comprised between 47 and 43 Ma, which largely overlaps the ages obtained for mylonitization (Figure 6). The spread observed toward younger ages (four points are in the range 43–45 Ma) may reflect partial reequilibration of analyzed phengite crystals during exhumation. The greenschist-facies overprinted foliated cataclasite (fabric B, sample #60b) from the DBT yields younger ages in the range 40–43 Ma, which clearly postdates the end of mylonitic deformation. This result, combined with thermobarometric data and phengite composition [*Angiboust et al*., 2014a] (Figure 5a), indicates that the main stage of cataclasis along the DBT took place before 42 Ma at pressures higher than 0.8 GPa. Our results demonstrate that (i) most of the brittle deformation (including cataclasis and hydrofracturing) along the DBT proceeded at depths larger than 30 km during the subduction event and not during late exhumation (as first proposed by *Wust and Silverberg* [1989]) and (ii) brittle and ductile deformation largely overlap in time and space in the hanging wall of the DBT.

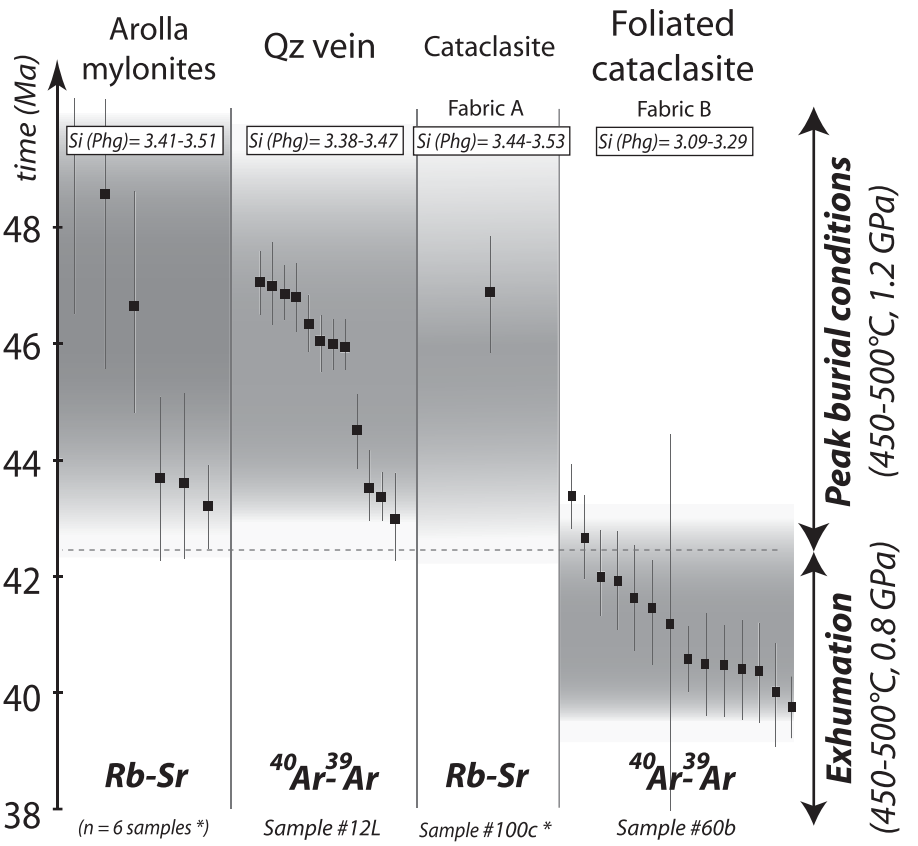

Figure 6. Results of geochronological investigations using in situ ^{40}Ar-^{39}Ar geochronology on phengite and Rb-Sr geochronology (*: data from *Angiboust et al.* [2014a]). The foliated greenschist facies cataclasite (sample #60b) exhibits the youngest ages indicating that high-pressure cataclasis occurred before 41 Ma, most likely between 48 and 42 Ma. The spread in ^{40}Ar-^{39}Ar ages might be related to variable degree of exhumation-related metamorphic reequilibration of phengite crystals. This figure shows that brittle (samples #100c, #12L, and #60b) and ductile deformation (see Rb-Sr ages for Arolla mylonites in *Angiboust et al.* [2014a]) apparently overlap in time in the DBT region.

5. Discussion

5.1. Genesis and Significance of DBT Cataclasites

Our field and petrological observations document the existence of multiple generations of brittle events with distinct microstructural expression. Semibrittle to brittle deformation responsible for fabric A formation took place first within a cool, prograde regime as attested by the coeval presence of Mg-riebeckite, rutile and high-silica phengite crystals (Figure 3c; T = 400–450°C, P = 1.2–1.4 GPa) [*Ayrton et al.*, 1982; *Angiboust et al.*, 2014a; *Manzotti et al.*, 2014, and references therein; Strøm, unpublished MS thesis, 1990]. The mineral modal difference between fabrics A and B (in particular the absence of blue amphibole) does not necessarily indicate a pressure drop. The apparent greenschist facies overprint visible within fabric B may reflect a moderate temperature increase (50–100°C; see the P-T path in Figure 2b) due to the warming of the Arolla slice after underplating or it may also be related to the Ca metasomatic overprint affecting foliated cataclasites [*Evans*, 1990; see also *Halama and Konrad-Schmolke*, 2015] (Figure 5b). The P-T-time path obtained on overprinted, foliated cataclasites (sample #60b; 40–43 Ma; 460–520°C; 0.7–0.9 GPa; Figure 2b) [*Angiboust et al.*, 2014a] indicates that cataclasis leading to the genesis of fabric B took place before 42 Ma at depths larger than 20 km (Figure 6). The finding of recrystallized, high-silica phengite crystals (Si = 3.4–3.5; Figure 5a) within fabric B matrix independently confirms that peak mylonitization, A as well as B-type cataclasis were largely coeval at depth, under lithostatic pressures comprised between 1.1 and 1.3 GPa (see phengite Si isopleths distribution in Figure 2b). We therefore emphasize that A-type and B-type fabrics formed contemporaneously with mylonitic deformation when the DBT was occupying a subduction interface position (42–48 Ma; depths of 30–40 km; Figure 6) and not during exhumation-related younger deformation. We also emphasize that the vein networks and the DBT foliated cataclasites were both affected by the km scale

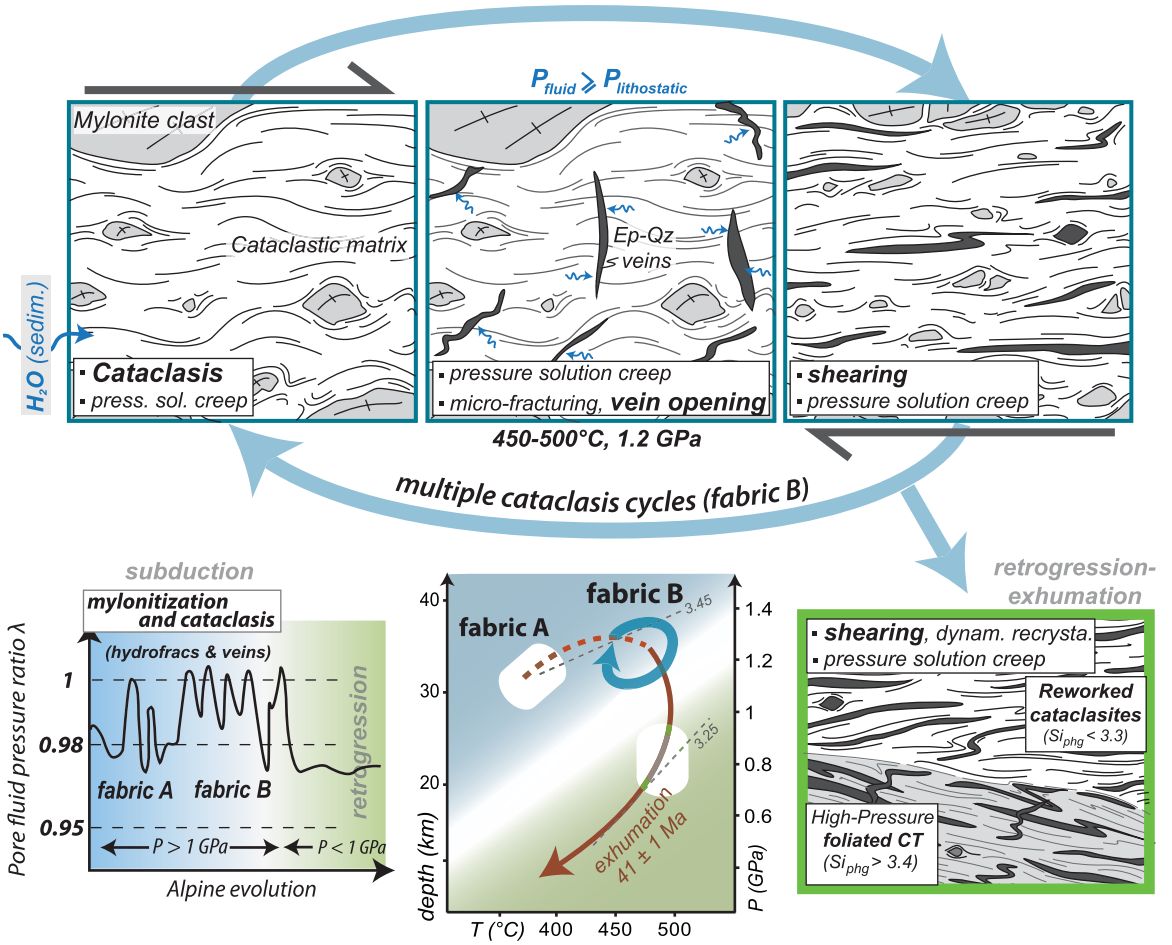

Figure 7. Conceptual model illustrating the cyclic nature of deformation within DBT rocks including cataclasis, vein opening, overprinting of cataclasites, and reorientation of veins. Transient supralithostatic pore fluid pressure ratios ($\lambda > 1$) may have led to vein opening during deformation, cutting through both fabrics A and B. Later, exhumation-related ductile reworking of brittle microstructures leads to partial retrogression of these brittle fabrics.

backfolds associated with the collisional "Mischabel phase" in this region at circa 38 Ma [e.g., *Markley et al.*, 1998; *Ring*, 1995], thus confirming that fabrics A and B originate from deep Alpine deformation and not from shallow, collisional-related overprint associated with late alpine stages and orogenic crust thickening. Note that the relatively good preservation of the high-pressure memory within A-type fabrics may also indicate that the shear zone responsible for their formation has been abandoned and therefore was shielded from the exhumation-related metamorphic overprint affecting B-type foliated cataclasites, closer to the basal contact with Tsaté complex rocks.

The presence of the more than 50 m thick, foliated cataclasite network observed along the DBT hanging wall (Figure 2c; fabric B) suggests the past existence of an extremely high number of fracturing events accommodating large amounts of cumulated strain, as it is expected for a subduction interface setting [e.g., *Carver and Plafker*, 2008]. Crosscutting relationships showing (i) multiple cataclasis events of Arolla gneiss mylonites and (ii) ductile reworking of quartz-clinozoisite veins and the development of crystal-preferred orientation within quartz-rich levels point to the presence of complex and multiple switches which are characteristic of the brittle-ductile transition [*Handy and Brun*, 2004; *Hirth and Beeler*, 2015] (Figure 7). The observed dynamic recrystallization overprint of the cataclastic fabric may reveal the existence of lateral variations in strain rate allowing both mechanisms to compete during the same time window. However, the multiple opening and the reorientation of quartz-clinozoisite veins tend to suggest that cataclasis and foliation overprint were rather sequential.

The opening of multiple quartz or quartz-clinozoisite-filled veins (Figure 4d) also sheds light on the past existence of transient highs in pore fluid pressures up to lithostatic values during each deformation cycle ($\lambda \geq 1$)

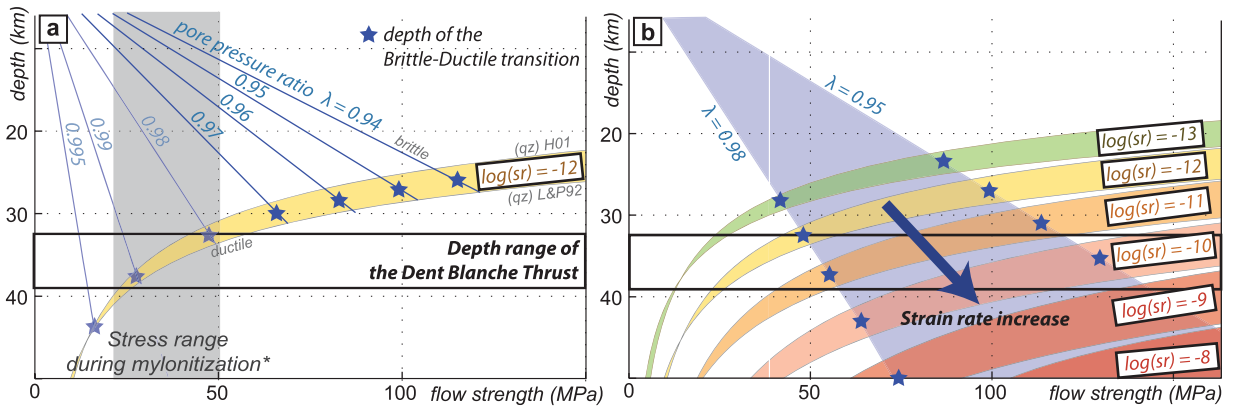

Figure 8. (a) Rheological profile calculated for a fixed strain rate of 10^{-12} s^{-1} (see text for calculation details) using the quartz flow laws from *Luan and Paterson* [1992, L&P92] and *Hirth et al*. [2001, H01]. Frictional Byerlee envelope is calculated using an average friction coefficient of 0.7 for various pore fluid pressure ratio values. Stress estimates based on recrystallized quartz piezometry (grey shaded area) have been calculated following [*Stipp and Tullis*, 2003]. (b) Rheological envelope calculated for various strain rates and for pore fluid pressures comprised between 0.95 and 0.98. Beyond uncertainties related to regional strain rate variations and friction coefficient values, this figure demonstrates that a strain rate increase of 1–2 orders of magnitude is sufficient to switch from the ductile to the brittle deformation regime under these conditions.

[e.g., *Sibson et al*., 1988]. These veins, together with ubiquitous pressure-solution fringes along the foliation, attests of the systematic presence of a fluid phase during all deformation stages recorded by both A-type and B-type foliated cataclasites (Figure 7). Porosity collapse associated with compaction and periodic changes in the main stress axis probably resulted in vein opening and vein filling at various angles with respect to the main cataclastic foliation [e.g., *Magee and Zoback*, 1993; *Sibson*, 1990].

Rheological envelope calculations, which are often used to localize the depth of the brittle-ductile transition for various settings and/or rock compositions [e.g., *Bürgmann and Dresen*, 2008], have been performed on DBT mylonites considering two flow laws for quartz and a strain rate of 10^{-12} s^{-1} (Figure 8a). This strain rate, considered as the average steady state strain rate occurring during mylonitization, has been calculated assuming distributed deformation along a 1 km thick shear zone (i.e., the subduction interface shear zone) and a convergence velocity of 3 cm/yr [e.g., *Yamato et al*., 2007]. The stress range during mylonitization (20–50 MPa) has been calculated using the quartz paleo-piezometer of *Stipp and Tullis* [2003] assuming that dislocation-creep is the dominant deformation process during mylonitization [*Handy*, 1989; *Menegon et al*., 2008] and considering a dynamically recrystallized quartz grain size distribution of 30–70 μm (see supporting information). Our results show that plastic deformation of quartz-rich DBT mylonites is possible in this case only if the pore fluid pressure to overburden ratio is lower than 0.98 (Figure 8a). In order to assess the potential role of strain rate variation on the genesis of cataclastic deformation, we also calculated the shape of the rheological envelope for various strain rates (between 10^{-8} and 10^{-13} s^{-1}; Figure 8b). Our calculations indicate that, for high pore fluid pressure ratios (in the range 0.95–0.98) based on *Lamb* [2006] and *Seno* [2009], it is possible to switch from plastic to brittle behavior by increasing the strain rate at least by 2 orders of magnitude (from 10^{-12} s^{-1} to 10^{-10} s^{-1} and higher). These considerations together with microstructural observations demonstrate that the structure of these foliated cataclasite domains cannot be achieved only by hydrofracturing processes associated with slight oscillations in λ values from 0.98 to 1. Geophysical observations in active subduction zones indeed show that pore fluid pressure ratios of 1 promote decoupling and stable slip rather than slip at seismic strain rates [e.g., *Audet et al*., 2009; *Moreno et al*., 2014]. The conjunction of elevated pore fluid pressures together with a local strain rate increase therefore constitutes the most plausible explanation to trigger brittle deformation and generate the cataclastic networks visible along the DBT hanging wall at temperatures and depths where ductile deformation should normally prevail. Note that the absence of multiple, crosscutting vein generations within fabric A cataclasites suggests that the pore fluid pressure may have been slightly lower than within the networks where fabric B developed (Figure 9, inset). This difference may reflect the existence of a pore fluid pressure gradient in the former subduction hanging wall, with the highest pressures on the subduction fault itself, at the contact with the underlying, dehydrating metasediments. It is finally important to recall that our stress and strain rate estimates likely reflect steady state or static conditions, while fluid pressures may well undergo

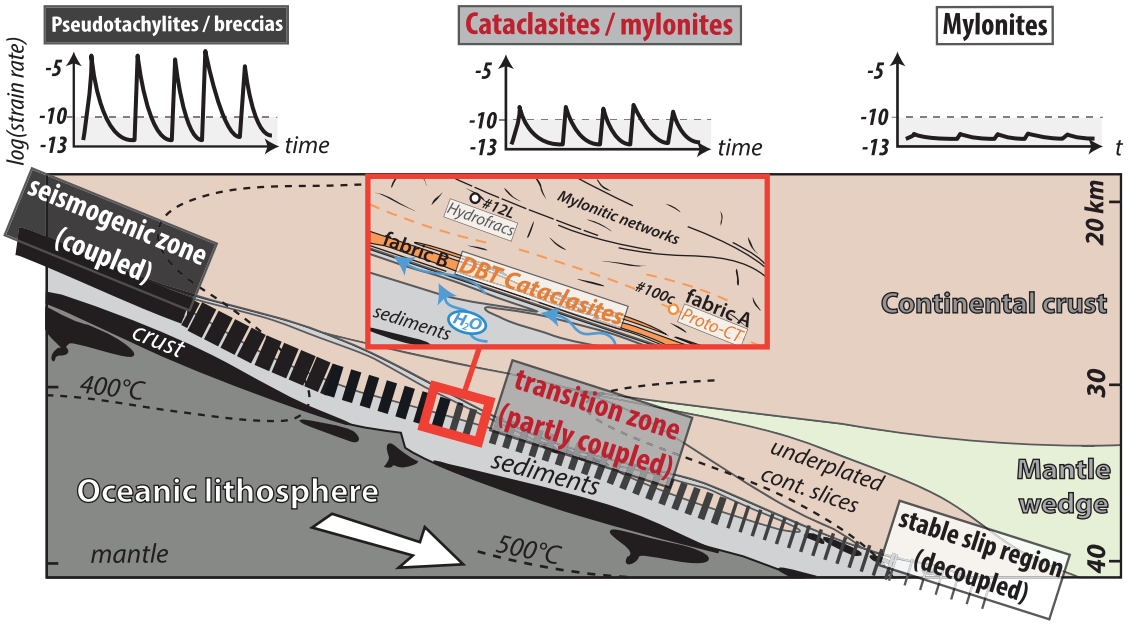

Figure 9. Sketch (not to scale) showing the Alpine subduction interface at 45 Ma and the distribution of the three main deformation patterns from the shallower, locked seismogenic zone to the deeper, decoupled region where plastic deformation dominates. Transient strain rate increase in the transition zone, coupled with very high pore fluid pressures trigger the genesis of brittle deformation in the subduction hanging wall. The abundance of fluids in this region of the plate interface can be explained by metamorphic dehydration reactions taking place in the oceanic plate and in particular in the metasedimentary material which is the main fluid source according to our geochemical results.

rapid change under dynamic conditions such as thermal pressurization [e.g., *Wibberley and Shimamoto*, 2005] or decompression boiling [e.g., *Caine et al.*, 2010] leading to very short-lived, local, quasi-lithostatic fluid pressure conditions (now recorded in the field by hydrofractures and vein systems; Figure 3b).

5.2. Fluid-Rock Processes Along the Subduction Interface

Seismological results indicate that the plate interface in the transition zone has very low permeabilities, thus maintaining high pore fluid pressures [e.g., *Audet et al.*, 2009; *Peacock et al.*, 2011; *Moreno et al.*, 2014]. Field, petrological, and geochemical investigations in the DBT region provide an excellent insight on fluid distribution and migration processes in this segment of the subduction interface (Figure 9). Three arguments support the idea that the fluids observed within DBT foliated cataclasites were externally derived, mainly from the underlying oceanic plate metasediments during progressive subduction-related dehydration. First, the syn-kinematic growth of pyrite within DBT fabrics A and B indicates the infiltration of sulfur-bearing fluids, most likely derived from the breakdown of the organic matter contained in oceanic sedimentary material [e.g., *Alt et al.*, 1993]. Second, strontium isotopic signatures of DBT foliated cataclasites and epidote veins from fabric B exhibit a range of values which matches the signature obtained for the underlying sediments (Figure 5c). Lastly, the enrichment in calcium associated with epidote-vein formation attests of the infiltration of an external Ca-rich fluid, also likely derived from the sediments, as they commonly contain up to 30 wt % CaO, mainly as calcium carbonate [e.g., *Garofalo*, 2012]. *Ague and Nicolescu* [2014] have shown that calcium carbonate progressively dissolves with burial in subduction zone environments, thus permitting the release of Ca^{2+} in the aqueous phase which circulates through the porosity generated during cataclasis along the DBT (Figure 9, inset; see also discussion in *Cook-Kollars et al.*, 2014). The fact that hydrofracture networks in the subduction hanging wall are confined to the first hundreds of meters above the DBT also suggests that expelled fluids, via prograde metamorphic reactions in the underlying oceanic lithosphere and associated sediments, mostly migrate parallel to the plate interface along anisotropic, advected within highly sheared deformation networks [e.g., *Kawano et al.*, 2011; *Angiboust et al.*, 2014b].

5.3. Highlighting Geophysical Observations

By shedding light on interplate deformation at strain rates comprised between seismic (10^{-1} to 10^{-3} s^{-1}) and regional-scale values (10^{-12} s^{-1}), the DBT region provides a unique opportunity to understand the

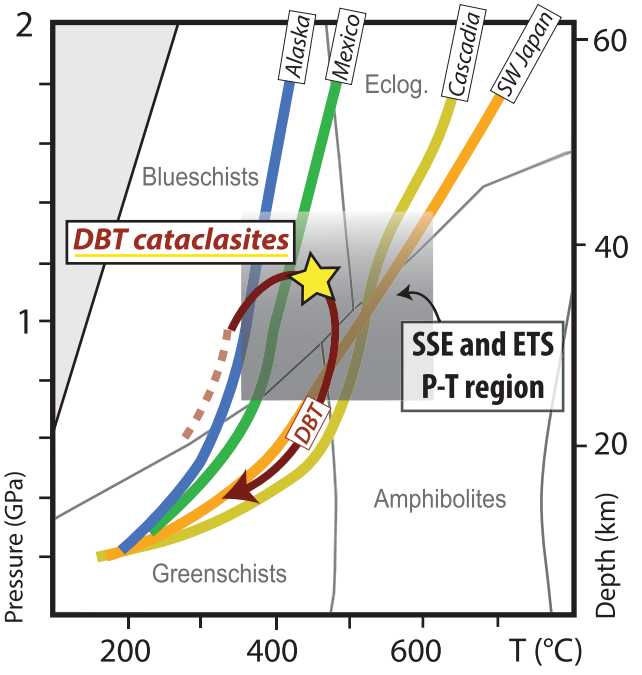

Figure 10. Pressure-Temperature diagram showing the predicted P-T path for the subduction interface for various subduction zones where episodic tremors and other slow slip phenomena have been reported (Japan, Cascadia, and Alaska thermal structure from *Abers et al.* [2013]; Mexico from *Currie et al.* [2002]). The P-T range for slow slip phenomena includes data from *Hayman and Lavier* [2014, and references therein] and *Fu and Freymueller* [2013] observations.

geometry, the rheology and the internal organization of structures responsible for interplate deformation between 30 and 40 km depth in the "transition zone," i.e., near the base of the seismogenic zone (Figure 9). The apparent absence of pseudotachylites within DBT gneisses suggests that the depth window exposed in the DBT region experienced a deformation regime which strongly differs from classical, cooler midcrustal seismicity as reported by previous authors for shallower segments of the Alpine subduction interface ($T < 350°C$) [*Bachmann et al.*, 2009, and references therein; see also *Meneghini et al.*, 2010; *Fagereng and Toy*, 2011]. While this may be due to elevated temperatures and/or to slip velocities too low for friction melting, it may well be also due to the presence of a fluid at near-lithostatic pressure. The discovery of these brittle networks in the DBT region demonstrates that transition zone deformation, which is normally dominated by crystal-plastic deformation processes at plate convergence velocities (i.e., mylonitization) and 450–500°C can locally exhibit a brittle deformation regime under near-lithostatic pore fluid pressures as a consequence of strain rate increase below and in the hanging wall of the subduction interface (Figure 8b) [see also *Hobbs et al.*, 1986; *Mancktelow*, 2006; *White*, 2012, and references therein].

Recent studies employing GPS allow monitoring small magnitude transient slip events and constraining the displacement along specific subduction interface segments in the transition zone during interseismic or postseismic stages of the seismic cycle [e.g., *Bedford et al.*, 2013]. Slip mechanisms and kinematics are highly variable in space and time, and often related to fluid transport or fluid production [e.g., *Ito et al.*, 2007; *Peacock et al.*, 2011]. They range over a broad spectrum from discrete afterslip patterns to slow slip events and transient episodic tremors (e.g., Japan: *Ozawa et al.* [2002]; Alaska: *Fu and Freymueller* [2013]; and Chile: *Bedford et al.* [2013]).

The DBT cataclasites can be best explained by two different slip patterns reported by these geophysical and geodetic studies of the transition zone: (i) afterslip displacement following megathrust rupture or (ii) slow slip phenomena. In the first case, the transient strain rate increase and the associated cataclastic cycles would represent the deep response of the transition zone to a specific stage of the seismic cycle taking place higher up along the seismogenic portion of the subduction interface (Figure 9). Cataclastic deformation would then correlate with coseismic to postseismic deformation higher up along the interface. In that case, the foliation of cataclasites with compaction and sealing of the rock would be the record of subsequent interseismic deformation at lower strain rates, taking place in the time frame between two megathrust earthquakes. In the second case, the transient highs in strain rates reported for DBT cataclasites could be seen as the field evidence of deformation associated with slow slip events or other transient slips, generally localized along the subduction interface at this depth range itself [e.g., *Shelly et al.*, 2006; see also *Fagereng et al.*, 2014].

Pressure-Temperature conditions estimated for the cataclasis events (in particular fabric B cataclasites) along the DBT fall into the P-T region where ETS and SSE are observed in subduction zones worldwide [see also *Hayman and Lavier*, 2014] (Figure 10). *Segall et al.* [2010] calculated that displacements during slow

transients occurring along the Cascadia margin are on the order of 2 cm at slip velocities of 10^{-8} m/s. Very similar slip patterns have been observed for the Hikurangi (NZ) and Central Japan subduction zones [*Miyazaki et al.*, 2006; *Wallace and Beavan*, 2010]. These examples of slow slip transients, calculated considering slip on a planar structure, yield strain rates comprised between 10^{-7} and 10^{-8} s^{-1}. Note that these estimates may be decreased by 1 or 2 orders of magnitude if, in nature, slip is distributed within a rock volume and not localized on a planar structure. Our calculations indicate that, for transient events rooted within a quartz-dominated material, brittle deformation should prevail under strain rates higher than $\sim 10^{-10}$ s^{-1}, most presumably via cataclastic faulting as visible in the DBT region (Figure 8). A similar faulting mechanism could also have persisted in the underlying oceanic sediments even though chances to preserve evidence for brittle deformation are lesser due to continuous reworking of structures by solution-precipitation creep during subduction and, later on, during exhumation-related deformation.

In any case, our results demonstrate that high pore fluid pressures, with λ values probably around 0.98, are mandatory to generate brittle deformation in the transition zone, in agreement with geophysical studies reporting particularly high Vp/Vs ratios in this region [e.g., *Peacock et al.*, 2011; *Moreno et al.*, 2014]. These very high pore fluid pressures during cataclasis are believed to maintain the effective normal stress down to values lower than 10 MPa, i.e., always close to failure conditions [e.g., *Peacock et al.*, 2011]. However, if pore fluid pressures were permanently lithostatic ($\lambda = 1$), the level of stress of the plate interface would drop to values near to zero and stable slip rather than transient slip would proceed in the transition zone region. Our results therefore demonstrate that transient shearing (and associated increased deformation rates) under λ values fluctuating between 0.95 and 1 constitutes the most likely conditions to trigger unstable, transient slip in the transition zone region.

6. Conclusions

The Dent Blanche Thrust in Western Alps, which corresponds to the hanging wall of an ancient subduction interface zone, exposes foliated cataclastic networks at the base of a unit of mylonitized orthogneisses from the upper continental plate. These networks formed during Alpine subduction between 42 and 48 Ma, at depths comprised between 30 and 40 km and under temperatures of 400–500°C. Field and microstructural observations revealed the existence of multiple switches between ductile and brittle deformation patterns. Numerous clinozoisite-quartz vein generations, pressure-solution seams, and strontium isotopic signatures indicate the past existence of a complex hydromechanical system, where Ca-rich fluids, derived from the underlying metasediments, repeatedly infiltrated the DBT region. Foliated cataclasite networks from the DBT hanging wall are interpreted as the record of transient strain rate increase in the transition zone region, near the downdip end of the seismogenic zone. On one hand, this brittle deformation may correspond to the deep afterslip response after a megathrust earthquake breaking the whole seismogenic zone higher up. On the other hand, these brittle networks could also be viewed as the rock record of slow slip phenomena as they apparently formed in the depth range where these events are reported by geophysical studies. In any case, we emphasize that the DBT region constitutes a unique target to image and understand deformation processes and fluid-rock interactions in the transition zone of subduction interfaces.

Acknowledgments
The authors thank Luiz Morales (GFZ) for his assistance for grain size distribution measurements at the EBSD and Roland Oberhänsli (Uni. Potsdam) for insightful discussions. Vincent Bettler is acknowledged for technical assistance to access the outcrops. H. Austrheim and an anonymous reviewer are acknowledged for insightful comments and suggestions. S.A. thanks the A. von Humboldt foundation for a postdoctoral fellowship which made this study possible. Data supporting this work are available as online supporting information. Any other data can be requested to the first author by email.

References

Abers, G. A., J. Nakajima, P. E. van Keken, S. Kita, and B. R. Hacker (2013), Thermal-petrological controls on the location of earthquakes within subducting plates, *Earth Planet. Sci. Lett.*, *369*, 178–187.

Agard, P., L. Jolivet, and B. Goffe (2001), Tectonometamorphic evolution of the Schistes Lustres Complex: Implications for the exhumation of HP and UHP rocks in the Western Alps, *Bull. Soc. Geol. Fr.*, *172*(5), 617–636.

Ague, J. J., and S. Nicolescu (2014), Carbon dioxide released from subduction zones by fluid-mediated reactions, *Nat. Geosci.*, *7*, 355–360.

Alt, J. C., W. C. Shanks III, and M. C. Jackson (1993), Cycling of sulfur in subduction zones: The geochemistry of sulfur in the Mariana Island Arc and back-arc trough, *Earth Planet. Sci. Lett.*, *119*(4), 477–494.

Andersen, T. B., H. Austrheim, N. Deseta, P. Silkoset, and L. D. Ashwal (2014), Large subduction earthquakes along the fossil Moho in Alpine Corsica, *Geology*, *42*(5), 395–398.

Angiboust, S., P. Agard, P. Yamato, and H. Raimbourg (2012), Eclogite breccias in a subducted ophiolite: A record of intermediate-depth earthquakes?, *Geology*, *40*(8), 707–710.

Angiboust, S., J. Glodny, O. Oncken, and C. Chopin (2014a), In search of transient subduction interfaces in the Dent Blanche-Sesia Tectonic System (W. Alps), *Lithos*, *205*, 298–321.

Angiboust, S., T. Pettke, J. C. De Hoog, B. Caron, and O. Oncken (2014b), Channelized fluid flow and eclogite-facies metasomatism along the subduction shear zone, *J. Petrol.*, *55*(5), 883–916.

Audet, P., M. G. Bostock, N. I. Christensen, and S. M. Peacock (2009), Seismic evidence for overpressured subducted oceanic crust and megathrust fault sealing, *Nature*, *457*(7225), 76–78.
Ayrton, E., C. Bugnon, T. Haarpaintner, M. Weidmann, and E. Frank (1982), Géologie du front de la nappe de la Dent Blanche dans la région des Monts-Dolins, Valais, *Eclogae Geol. Helv.*, *75*(2), 269–286.
Bachmann, R., O. Oncken, J. Glodny, W. Seifert, V. Georgieva, and M. Sudo (2009), Exposed plate interface in the European Alps reveals fabric styles and gradients related to an ancient seismogenic coupling zone, *J. Geophys. Res.*, *114*, B05402, doi:10.1029/2008JB005927.
Ballèvre, M., and O. Merle (1993), The combin fault—Compressional reactivation of a late cretaceous-early tertiary detachment fault in the Western Alps, *Schweiz. Mineral. Petrogr. Mitt.*, *73*(2), 205–227.
Bedford, J., et al. (2013), A high-resolution, time-variable afterslip model for the 2010 Maule Mw = 8.8, Chile megathrust earthquake, *Earth Planet. Sci. Lett.*, *383*, 26–36.
Bürgmann, R., and G. Dresen (2008), Rheology of the lower crust and upper mantle: Evidence from rock mechanics, geodesy, and field observations, *Annu. Rev. Earth Planet. Sci.*, *36*(1), 531–561.
Caine, J. S., R. L. Bruhn, and C. B. Forster (2010), Internal structure, fault rocks, and inferences regarding deformation, fluid flow, and mineralization in the seismogenic Stillwater normal fault, Dixie Valley, Nevada, *J. Struct. Geol.*, *32*(11), 1576–1589.
Carver, G., and G. Plafker (2008), Paleoseismicity and neotectonics of the Aleutian subduction zone—An overview, in *Active Tectonics and Seismic Potential of Alaska*, edited by J. T. Freymueller et al., pp. 43–63, AGU, Washington, D. C.
Cook-Kollars, J., G. E. Bebout, N. C. Collins, S. Angiboust, and P. Agard (2014), Subduction zone metamorphic pathway for deep carbon cycling: I. Evidence from HP/UHP Metasedimentary Rocks, Italian Alps, *Chem. Geol.*, *386*, 31–48.
Currie, C. A., R. D. Hyndman, K. Wang, and V. Kostoglodov (2002), Thermal models of the Mexico subduction zone: Implications for the megathrust seismogenic zone, *J. Geophys. Res.*, *107*(B12), 2370, doi:10.1029/2001JB000886.
Evans, B. W. (1990), Phase relations of epidote-blueschists, *Lithos*, *25*(1), 3–23.
Fagereng, Å., and V. G. Toy (2011), Geology of the earthquake source: An introduction, *Geol. Soc. Spec. Publ.*, *359*(1), 1–16.
Fagereng, Å., G. W. Hillary, and J. F. Diener (2014), Brittle-viscous deformation, slow slip, and tremor, *Geophys. Res. Lett.*, *41*, 4159–4167, doi: 10.1002/2014GL060433.
Frank, W. B., N. M. Shapiro, A. L. Husker, V. Kostoglodov, H. S. Bhat, and M. Campillo (2015), Along-fault pore-pressure evolution during a slow-slip event in Guerrero, Mexico, *Earth Planet. Sci. Lett.*, *413*, 135–143.
Fu, Y., and J. T. Freymueller (2013), Repeated large slow slip events at the southcentral Alaska subduction zone, *Earth Planet. Sci. Lett.*, *375*, 303–311.
Garofalo, P. S. (2012), The composition of Alpine marine sediments (Bündnerschiefer Formation, W Alps) and the mobility of their chemical components during orogenic metamorphism, *Lithos*, *128*, 55–72.
Gebauer, D. (1999), Alpine geochronology of the Central and Western Alps: New constraints for a complex geodynamic evolution, *Schweiz. Mineral. Petrogr. Mitt.*, *79*(1), 191–208.
Glodny, J., H. Austrheim, J. F. Molina, A. I. Rusin, and D. Seward (2003), Rb/Sr record of fluid-rock interaction in eclogites: The Marun-Keu complex, Polar Urals, Russia, *Geochim. Cosmochim. Acta.*, *67*(22), 4353–4371.
Hacker, B. R., S. M. Peacock, G. A. Abers, and S. D. Holloway (2003), Subduction factory: 2. Are intermediate-depth earthquakes in subducting slabs linked to metamorphic dehydration reactions?, *J. Geophys. Res.*, *108*(B1), 2030, doi:10.1029/2001JB001129.
Halama, R., and M. Konrad-Schmolke (2015), Retrograde metasomatic effects on phase assemblages in an interlayered blueschist-greenschist sequence (Coastal Cordillera, Chile), *Lithos*, *216*, 31–47.
Handy, M. R. (1989), Deformation regimes and the rheological evolution of fault zones in the lithosphere: The effects of pressure, temperature, grainsize and time, *Tectonophysics*, *163*(1), 119–152.
Handy, M. R., and J. P. Brun (2004), Seismicity, structure and strength of the continental lithosphere, *Earth Planet. Sci. Lett.*, *223*(3), 427–441.
Hayman, N. W., and L. L. Lavier (2014), The geologic record of deep episodic tremor and slip, *Geology*, *42*(3), 195–198.
Hirth, G., and N. M. Beeler (2015), The role of fluid pressure on frictional behavior at the base of the seismogenic zone, *Geology*, *43*(3), 223–226.
Hirth, G., C. Teyssier, and J. W. Dunlap (2001), An evaluation of quartzite flow laws based on comparisons between experimentally and naturally deformed rocks, *Int. J. Earth Sci.*, *90*(1), 77–87.
Hobbs, B. E., A. Ord, and C. Teyssier (1986), Earthquakes in the ductile regime?, *Pure Appl. Geophys.*, *124*(1–2), 309–336.
Ito, Y., K. Obara, K. Shiomi, S. Sekine, and H. Hirose (2007), Slow earthquakes coincident with episodic tremors and slow slip events, *Science*, *315*(5811), 503–506.
Kawano, S., I. Katayama, and K. Okazaki (2011), Permeability anisotropy of serpentinite and fluid pathways in a subduction zone, *Geology*, *39*(10), 939–942.
Kodaira, S., T. Iidaka, A. Kato, J. O. Park, T. Iwasaki, and Y. Kaneda (2004), High pore fluid pressure may cause silent slip in the Nankai Trough, *Science*, *304*(5675), 1295–1298.
Lamb, S. (2006), Shear stresses on megathrusts: Implications for mountain building behind subduction zones, *J. Geophys. Res.*, *111*, B07401, doi:10.1029/2005JB003916.
Liu, Y., and J. R. Rice (2007), Spontaneous and triggered aseismic deformation transients in a subduction fault model, *J. Geophys. Res.*, *112*, B09404, doi:10.1029/2007JB004930.
Luan, F. C., and M. S. Paterson (1992), Preparation and deformation of synthetic aggregates of quartz, *J. Geophys. Res.*, *97*(B1), 301–320.
Magee, M. E., and M. D. Zoback (1993), Evidence for a weak interplate thrust fault along the northern Japan subduction zone and implications for the mechanics of thrust faulting and fluid expulsion, *Geology*, *21*(9), 809–812.
Mancktelow, N. S. (2006), How ductile are ductile shear zones?, *Geology*, *34*(5), 345–348.
Manzotti, P., M. Zucali, M. Ballevre, M. Robyr, and M. Engi (2014), Geometry and kinematics of the Roisan-Cignana Shear Zone, and the orogenic evolution of the Dent Blanche Tectonic System (Western Alps), *Swiss J. Geosci.*, *107*(1), 23–47.
Markley, M. J., C. Teyssier, M. A. Cosca, R. Caby, J. C. Hunziker, and M. Sartori (1998), Alpine deformation and $^{40}Ar/^{39}Ar$ geochronology of synkinematic white mica in the Siviez-Mischabel Nappe, western Pennine Alps, Switzerland, *Tectonics*, *17*(3), 407–425.
Marthaler, M., and G. M. Stampfli (1989), Les Schistes lustrés à ophiolites de la nappe du Tsaté: Un ancien prisme d'accrétion issu de la marge active apulienne?, *Schweiz. Mineral. Petrogr. Mitt.*, *69*(2), 211–216.
Mazurek, M. (1986), Structural evolution and metamorphism of the Dent Blanche nappe and the Combin zone west of Zermatt (Switzerland), *Eclogae Geol. Helv.*, *79*, 41–56.
Meneghini, F., G. Di Toro, C. D. Rowe, J. C. Moore, A. Tsutsumi, and A. Yamaguchi (2010), Record of mega-earthquakes in subduction thrusts: The black fault rocks of Pasagshak Point (Kodiak Island, Alaska), *Geol. Soc. Am. Bull.*, *122*(7–8), 1280–1297.
Menegon, L., G. Pennacchioni, R. Heilbronner, and L. Pittarello (2008), Evolution of quartz microstructure and c-axis crystallographic preferred orientation within ductilely deformed granitoids (Arolla unit, Western Alps), *J. Struct. Geol.*, *30*, 1332–1347.

Miyazaki, S. I., P. Segall, J. J. McGuire, T. Kato, and Y. Hatanaka (2006), Spatial and temporal evolution of stress and slip rate during the 2000 Tokai slow earthquake, *J. Geophys. Res.*, *111*, B03409, doi:10.1029/2004JB003426.
Moreno, M., C. Haberland, O. Oncken, A. Rietbrock, S. Angiboust, and O. Heidbach (2014), Locking of the Chile subduction zone controlled by fluid pressure before the 2010 earthquake, *Nat. Geosci.*, *7*(4), 292–296.
Oleskevich, D. A., R. D. Hyndman, and K. Wang (1999), The updip and downdip limits to great subduction earthquakes: Thermal and structural models of Cascadia, south Alaska, SW Japan, and Chile, *J. Geophys. Res.*, *104*(B7), 14,965–14,991.
Ozawa, S., M. Murakami, M. Kaidzu, T. Tada, T. Sagiya, Y. Hatanaka, H. Yarai, and T. Nishimura (2002), Detection and monitoring of ongoing aseismic slip in the Tokai region, central Japan, *Science*, *298*(5595), 1009–1012.
Peacock, S. M., and R. D. Hyndman (1999), Hydrous minerals in the mantle wedge and the maximum depth of subduction thrust earthquakes, *Geophys. Res. Lett.*, *26*(16), 2517–2520.
Peacock, S. M., and K. Wang (1999), Seismic consequences of warm versus cool subduction metamorphism: Examples from southwest and northeast Japan, *Science*, *286*(5441), 937–939.
Peacock, S. M., N. I. Christensen, M. G. Bostock, and P. Audet (2011), High pore pressures and porosity at 35 km depth in the Cascadia subduction zone, *Geology*, *39*(5), 471–474.
Peng, Z., and J. Gomberg (2010), An integrated perspective of the continuum between earthquakes and slow-slip phenomena, *Nat. Geosci.*, *3*(9), 599–607.
Pennacchioni, G., and A. Guermani (1993), The mylonites of the Austroalpine Dent Blanche nappe along the northwestern side of the Valpelline Valley (Italian Western Alps), *Mem. Sci. Geol.*, *45*, 37–55.
Ring, U. (1995), Horizontal contraction or horizontal extension? Heterogeneous Late Eocene and Early Oligocene general shearing during blueschist and greenschist facies metamorphism at the Pennine-Austroalpine boundary zone in the Western Alps, *Geol. Rundsch.*, *84*(4), 843–859.
Rogers, G., and H. Dragert (2003), Episodic tremor and slip on the Cascadia subduction zone: The chatter of silent slip, *Science*, *300*(5627), 1942–1943.
Rosenbaum, G., L. Menegon, J. Glodny, P. Vasconcelos, U. Ring, M. Massironi, and P. Nasipuri (2012), Dating deformation in the Gran Paradiso Massif (NW Italian Alps): Implications for the exhumation of high-pressure rocks in a collisional belt, *Lithos*, *144*, 130–144.
Scholz, C. H. (1998), Earthquakes and friction laws, *Nature*, *391*(6662), 37–42.
Segall, P., A. M. Rubin, A. M. Bradley, and J. R. Rice (2010), Dilatant strengthening as a mechanism for slow slip events, *J. Geophys. Res.*, *115*, B12305, doi:10.1029/2010JB007449.
Seno, T. (2009), Determination of the pore fluid pressure ratio at seismogenic megathrusts in subduction zones: Implications for strength of asperities and Andean-type mountain building, *J. Geophys. Res.*, *114*, B05405, doi:10.1029/2008JB005889.
Shelly, D. R., G. C. Beroza, S. Ide, and S. Nakamula (2006), Low-frequency earthquakes in Shikoku, Japan, and their relationship to episodic tremor and slip, *Nature*, *442*(7099), 188–191.
Sibson, R. H. (1977), Fault rocks and fault mechanisms, *J. Geol. Soc.*, *133*(3), 191–213.
Sibson, R. H. (1990), Faulting and fluid flow, in *Fluids in Tectonically Active Regimes of the Continental Crust, Short Course Handbook*, vol. 18, edited by B. E. Nesbitt, pp. 93–132, Mineral. Assoc. of Can., Vancouver.
Sibson, R. H., F. Robert, and K. H. Poulsen (1988), High-angle reverse faults, fluid-pressure cycling, and mesothermal gold-quartz deposits, *Geology*, *16*(6), 551–555.
Stipp, M., and J. Tullis (2003), The recrystallized grain size piezometer for quartz, *Geophys. Res. Lett.*, *30*(21), 2088, doi:10.1029/2003GL018444.
Tichelaar, B. W., and L. J. Ruff (1993), Depth of seismic coupling along subduction zones, *J. Geophys. Res.*, *98*(B2), 2017–2037.
Wada, I., and K. Wang (2009), Common depth of slab-mantle decoupling: Reconciling diversity and uniformity of subduction zones, *Geochem. Geophys. Geosyst.*, *10*, Q10009, doi:10.1029/2009GC002570.
Wallace, L. M., and J. Beavan (2010), Diverse slow slip behavior at the Hikurangi subduction margin, New Zealand, *J. Geophys. Res.*, *115*, B12402, doi:10.1029/2010JB007717.
Wheeler, J., and R. W. Butler (1993), Evidence for extension in the western Alpine orogen: The contact between the oceanic Piemonte and overlying continental Sesia units, *Earth Planet. Sci. Lett.*, *117*(3), 457–474.
White, J. C. (2012), Paradoxical pseudotachylyte—Fault melt outside the seismogenic zone, *J. Struct. Geol.*, *38*, 11–20.
Wibberley, C. A., and T. Shimamoto (2005), Earthquake slip weakening and asperities explained by thermal pressurization, *Nature*, *436*(7051), 689–692.
Wust, G. H., and D. S. Silverberg (1989), Northern Combin zone complex-Dent Blanche nappe contact: Extension within the convergent Alpine belt, *Schweiz. Mineral. Petrogr. Mitt.*, *69*(2), 251–259.
Yamato, P., P. Agard, E. Burov, L. Le Pourhiet, L. Jolivet, and C. Tiberi (2007), Burial and exhumation in a subduction wedge: Mutual constraints from thermomechanical modeling and natural P-T-t data (Schistes Lustrés, western Alps), *J. Geophys. Res.*, *112*, B07410, doi:10.1029/2006JB004441.